Systemic Inflammation by Collagen-Induced Arthritis Affects the Progression of Age-Related Macular Degeneration Differently in Two Mouse Models of the Disease

Gloriane Schnabolk,[1] Elisabeth Obert,[1] Nirmal K. Banda,[2] and Bärbel Rohrer[1,3]

[1]Department of Ophthalmology, Medical University of South Carolina, Charleston, South Carolina, United States
[2]Division of Rheumatology, Department of Medicine, University of Colorado Anschutz Medical Campus, Aurora, Colorado, United States
[3]Ralph H. Johnson VA Medical Center, Division of Research, Charleston, South Carolina, United States

Correspondence: Gloriane Schnabolk, Department of Ophthalmology, Medical University of South Carolina, 167 Ashley Avenue, Charleston, SC 29425, USA; faith@musc.edu.

Received: May 28, 2020
Accepted: November 14, 2020
Published: December 8, 2020

Citation: Schnabolk G, Obert E, Banda NK, Rohrer B. Systemic inflammation by collagen-induced arthritis affects the progression of age-related macular degeneration differently in two mouse models of the disease. *Invest Ophthalmol Vis Sci.* 2020;61(14):11. https://doi.org/10.1167/iovs.61.14.11

Purpose. Age-related macular degeneration (AMD) shares similar risk factors and inflammatory responses with rheumatoid arthritis (RA). Previously, we identified increased risk for dry AMD among patients with RA compared to control subjects, using retrospective data analysis. In this current study, we investigate the role of systemic inflammation triggered in a murine model of arthritis on choroidal neovascularization and retinal pigment epithelium (RPE) degeneration mouse models.

Methods. Collagen-induced arthritis (CIA) was induced in C57BL/6J mice prior to laser-induced choroidal neovascularization (CNV; wet AMD model) or sodium iodate–induced retinal degeneration ($NaIO_3$; dry AMD model). CNV lesion size and retinal thickness were quantified by optical coherence photography (OCT), visual function was analyzed using optokinetic response and electroretinography, RPE morphology was examined by immunohistochemistry, and inflammatory gene expression was analyzed by quantitative PCR.

Results. CIA mice demonstrated decreased spatial acuity and contrast sensitivity, whereas no difference was observed in the RPE-generated c-wave. CNV lesion size was decreased in CIA mice. $NaIO_3$ decreased c-wave amplitude, as well as retinal thickness, which was augmented by CIA. $NaIO_3$ treatment resulted in loss of normal RPE hexagonal shape, which was further aggravated by CIA. Increased Cxcl9 expression was observed in the presence of CIA and CIA combined with AMD. Disease severity differences were observed between sexes.

Conclusions. Our data suggest systemic inflammation by CIA results in increased pathology in a dry AMD model, whereas it reduces lesions in a wet AMD model. These findings highlight the need for additional investigation into the role of secondary inflammation and sex-based differences on AMD.

Keywords: age-related macular degeneration, rheumatoid arthritis, choroidal neovascularization, optical coherence tomography

Age-related macular degeneration (AMD) is a multifactorial disease involving genetic variants (including but not limited to *CFH*,[1–4] *C2/CFB/SKIV2L*,[5,6] *ARMS2/HTRA1*,[7–9] and *C3*),[10] environmental risk factors including smoking[11] and diet,[12] and traits such as race[13] and sex.[14] As the leading cause of blindness among the elderly in the United States, AMD is estimated by the National Eye Institute of the National Institutes of Health to affect more than 3.5 million individuals by 2030.[15] AMD is characterized as either exudative, also known as wet AMD, or nonexudative, also known as dry AMD. Blindness from wet AMD is primarily the result of new blood vessel growth emanating from the choriocapillaris and breaking through into the retina, a process referred to as choroidal neovascularization (CNV). An estimated 15% to 20% of wet AMD cases are believed to be the result of retinal angiomatous proliferation, in which blood vessels from the retina invade the subretinal space.[16–18] Alternatively, dry AMD is the result of chronic degeneration, characterized by loss of retinal pigment epithelium (RPE), choriocapillaris, and photoreceptors, leading to thinning of the retina. With AMD onset typically occurring after age 60 years, it is likely that a number of these patients may also have preexisting systemic diseases. However, the contributions of a preexisting inflammatory disease on AMD progression are largely unknown. To date, comorbidities such as gout,[19] diabetes,[20] cardiovascular disease,[21] and myeloproliferative neoplasm[22] have been identified for AMD. In addition, we identified an increased risk of dry AMD

diagnosis among patients with rheumatoid arthritis (RA), along with an earlier time of diagnosis, through retrospective analysis of a Medicare patient database.[23] This study also identified an increased risk of AMD among female patients with RA compared to males. While reports linking an increased incidence of AMD among females in the general population are conflicting, a higher prevalence of females (65%) to males (35%) is diagnosed with AMD according to the 2010 National Eye Institute consensus.[15] Likewise, health care claims databases find that approximately 75% of patients with RA are females compared to ∼25% males.[24] Like AMD, RA is an inflammatory disease associated with, in part, an overactive complement system, increased levels of cytokines, and a persistent effector T-cell response. Both RA and AMD have altered levels of circulating factors B[5,25] and C3,[10,26] as well as increased deposition of the membrane attack complex,[27,28] in affected tissues. In addition, cytokines, including IL-6, IL-17, and TNF-α, are found to be elevated in both AMD[29–31] and RA.[32]

As RA, with its typical onset between the ages of 30 and 50 years, tends to precede AMD diagnosis, we question whether systemic inflammation could lead to increased AMD risk and faster disease progression. Medzhitov[33] suggested that parainflammation, a protective response having characteristics between basal and inflammatory states and geared toward maintaining tissue homeostasis, could be lost during prolonged or sustained stress generated by a chronic inflammatory disease. As we have observed an increased incidence of dry AMD in patients with RA, and as AMD and RA are found to be more prevalent in females, we sought to further analyze these questions within our analysis, using mouse models. Therefore, in this study, we investigate the role of a systemic disease on local inflammation in the eye using mouse models for AMD and RA in both male and female mice.

Materials and Methods

Animals

C57BL/6J mice were purchased from Jackson Laboratories (stock number 000664; Bar Harbor, ME, USA) and housed under a 12:12-hour light/dark cycle with access to food and water ad libitum. Experiments were performed in accordance with the ARVO Statement for the Use of Animals in Ophthalmic and Vision Research and were approved by the Medical University of South Carolina Institutional Animal Care and Use Committee.

Collagen-Induced Arthritis Model

Anesthetized (20 mg/kg xylazine and 80 mg/kg ketamine intraperitoneally) 8-week-old C57BL/6J mice were injected subcutaneously at the base of the tail with 100 µL of an emulsification of collagen type II (CII) from calf articular joints (2 mg/mL; Elastin Products Company, Owensville, MO, USA) and incomplete Freund's Adjuvant (Voigt Global Distribution, Lawrence, KS) containing heat-inactivated *Mycobacterium tuberculosis* (2 mg/mL; H37RA; Voigt Global Distribution) on days 0 and 21.[34] Arthritis developed 4 to 5 weeks after the first collagen injection and was monitored by the appearance of redness on the fore- and hindlimbs, as well as by ELISA analysis of IgG1 antibody responses to CII, as previously described.[35,36]

Optokinetic Responses

Visual acuity and contrast sensitivity were measured as previously described,[37,38] using the OptoMotry setup (Cerebral Mechanics, Lehtbridge, Alberta, Canada). Mice were placed on the center of an elevated pedestal surrounded by four computer monitors. Using OptoMotry software, stimulus gratings were displayed on the computer screens. Visual recordings of mouse head responses to rotating vertical grating were recorded through use of an overhead closed-circuit television camera. Visual acuity results were based on a constant speed of 12°/s and 100% contrast by means of a staircase procedure. Contrast sensitivity was recorded at a speed of 12°/s and a contrast threshold of 0.131 cycles per degree. The reciprocal of the contrast threshold was used to record contrast sensitivity as a percentage (0%–100%). A mean screen luminance of 52 cd m^{-2} was used for all optokinetic response (OKR) tests.

Electroretinography

Electroretinography (ERG) recordings to measure electrical responses of RPE (c-waves) were performed in control and collagen-induced arthritis (CIA) mice and 5 days after laser-induced CNV or 10 days after sodium iodate ($NaIO_3$) treatment. Mice were dark-adapted overnight, and the following day, mice were anesthetized as described above and pupils dilated (2.5% phenylephrine hydrochloric acid [HCl] and 1% atropine sulfate). Corneal loop electrodes were applied to the mouse eye with a drop of Goniovisc (Rancho Cucamonga, CA, USA) applied to maintain electrical contact between cornea and electrode. Needle electrodes were inserted into the scalp to provide reference and into the tail to provide ground. Response of c-waves was performed as previously described using the UTAS E-4000 System (LKC Technologies, Gaithersburg, MD, USA), with c-waves measured from the baseline to peak maximum in responses to a 100-cd*s mm^{-2} flash.[38,39]

OCT Analysis

Optical coherence tomography (OCT) measurements were performed following ERG analysis using the Bioptigen spectral-domain optical coherence tomography system (Bioptigen, Durham, NC, USA) as previously described.[40] Eyes were kept hydrated with sterile lubricant eye drops. Five days after laser-induced CNV, rectangular volume scan images set at 1.6 × 1.6 mm, consisting of 100 B scans (1000 A scans per B scan), were acquired. Using the en face fundus reconstruction tool, the cross-sectional area of each lesion was measured as previously described, with the axial interval positioned at the level of the RPE/choroid complex.[41] The hyporeflective area produced on the fundus image was measured with vertical calipers set at 0.1 mm using ImageJ software (Wayne Rasband, National Institutes of Health, Bethesda, MD, USA). Final lesion size was calculated based on the size of individual pixels (1.6 × 1.6 µm). Retinal structure was assessed 10 days following $NaIO_3$ treatment. The average of five separate scans (each consisting of 33 B scans, 1000 A scans per B scan) was taken to generate a high-resolution image by which to measure the thickness of individual retinal layers within the eye as previously described.[42] Scans were taken from the nasal quadrant, with measurements taken 350 µm from the optic disk.

Investigative Ophthalmology & Visual Science

Table 1. Quantitative RT-PCR Primer Sequences

Gene Name	Symbol	Forward Primer	Reverse Primer
Complement component 3	*C3*	5′-TCAGATAAGGAGGGGCACAA-3′	5′-ATGAAGAGGTACCCACTCTGGA-3′
Ionized calcium binding adaptor molecule 1	*Iba1*	5′-GTCCTTGAAGCGAATGCTGG-3’	5′-CATTCTCAAGATGGCAGATC-3′
Cluster of differentiation 68	*CD68*	5′-TGGATTGAGGAAGGAACTGG-3′	5′-GTAACGGCCTTTTTGTGAGG-3′
C-X-C motif chemokine ligand 9	*Cxcl9*	5′-TTTTGGGCATCATCTTCCTGG-3′	5′-GAGGTCTTTGAGGGATTTGTAGTGG-3′
C-X-C motif chemokine ligand 10	*Cxcl10*	5′-CCAAGTGCT GCC GTCATTTT-3′	5′-CTC AAC ACG TGG GCAGGATA-3′
Actin, β	*Actb*	5′-AGCTGAGAGGGAAATCATGC-3′	5′-ACCAGACAGCACTGTGTTG-3′
Acid ribosomal phosphoprotein P0	*36B4*	5′-TCACTGTGCCAGCTCAGAAC-3′	5′-AATTTCAATGGTGCCTCTGG-3′

Immunohistochemistry

Following removal of the lens, anterior structures, and retina, eyecups were fixed overnight at 4°C with 4% paraformaldehyde.[43] Eyecups were washed with 1× PBS prior to overnight incubation with blocking solution (10% normal goat serum and 0.4% Triton X-100 in Tris-buffered saline) containing ZO-1 antibody (1:200 cat. 61-7300; Invitrogen, Grand Island, NY, USA). Eyecups were washed and incubated with a secondary antibody (1:400 Alexa Fluor 488 goat anti-rabbit, cat. A-11008; Invitrogen). Four relaxing cuts were made to flatten the eyecups, which were then mounted to slides using Fluoromount (Southern Biotechnology Associates, Birmingham, AL, USA). Fluorescent microscopy (Zeiss, Thornwood, NY, USA) was used to image the flatmounts.

RPE Morphology

Images of ZO-1 staining of the peripheral region of RPE/choroid flatmounts were imported into ImageJ software for analysis. Images of equal size and exposure were used for comparison of RPE cell area and form factor in control and treated groups. Form factor was defined as the circularity (4π*area/perimeter^2) of each cell and determined using the shape descriptor settings under set measurements. As described by ImageJ, cells with values approaching 0.0 were indicative of an increasingly elongated shape, and a value of 1.0 equaled perfect circularity. Results were exported into GraphPad Prism software (GraphPad Software, La Jolla, CA, USA) for statistical analysis.

Laser-Induced Choroidal Neovascularization

Age-matched mice in the presence and absence of CIA were anesthetized (xylazine and ketamine, 20 and 80 mg/kg, respectively) and pupils dilated (one drop of 2.5% phenylephrine HCl and 1% atropine sulfate). Using argon laser photocoagulation (532 nm, 100-µm spot size, 0.1-second duration, 10 mW), four laser lesions were generated around the optic nerve of both eyes. Proper ruptured of Bruch's membrane was confirmed by visual bubble formation.[44,45]

$NaIO_3$-Induced Retinal Degeneration

To induce RPE cell death and loss of outer blood-retina barrier function followed by outer retina loss, CIA mice and age-matched control mice were treated by intraperitoneal injection of 50 mg/kg $NaIO_3$ (Sigma-Aldrich, St. Louis, MO, USA) diluted in 0.9% sterile sodium chloride.[46]

Quantitative RT-PCR

On day 6 following laser-induced CNV and day 11 following $NaIO_3$-induced retinal degeneration, individual RPE/choroid fractions were isolated from mice and stored at –80°C until use. RNA was isolated using the miRNEASY Kit (Qiagen, Valencia, CA, USA). Absorbance A260/A280 ratio (Take 3 Micro-Volume Plates; Biotek, Winooski, VT, USA) was used to measure the purity of RNA, and samples with measurements of 1.8 to 2.1 were used to generate first-strand cDNA (Qiagen). Using the Realplex 2 Mastercyler (Eppendorf, Hauppauge, NY, USA), PCR amplifications for genes of interest (Table 1) were performed as previously described.[47] Quantitative values were obtained using cycle number (Ct value) with values normalized to either β-actin or 36B4.[48]

Statistics

Data are presented as mean ± SEM and statistical analysis performed using GraphPad Prism software. Single comparisons were analyzed using unpaired *t*-tests. One-way ANOVA using Tukey's multiple comparison test was used to analyze multiple comparisons between one variable. Two-way ANOVA using Sidak's multiple comparison test was used to measure two variables between multiple groups. Significance was reported at $P \leq 0.05$.

Results

Functional Readouts and Retinal Morphology Following Collagen-Induced Arthritis

To determine ocular manifestations of CIA, structure/function tests were performed. OKR assessment indicated a significant decrease in spatial acuity in the CIA mice compared to controls (Fig. 1A; $P \leq 0.0001$). A large decrease was also observed in contrast sensitivity between control and CIA mice (Fig. 1B; $P \leq 0.001$). No significant difference was observed between CIA male and female mice for either spatial frequency tuning ($P = 0.1908$) or contrast sensitivity ($P = 0.9957$). However, female but not male mice were found to have a significant difference between control and CIA values for visual acuity ($P \leq 0.001$) and contrast sensitivity ($P \leq 0.05$). ERG c-wave analysis, documenting RPE function, revealed no changes in response between control and CIA mice (Fig. 1C; $P = 0.1126$) and no significant differences between male and female CIA mice ($P = 0.3849$). Nonetheless, male control mice in the absence of CIA exhibited a significant decrease in c-wave response when compared to female controls ($P \leq 0.05$). Retina and RPE morphology were evaluated by fundus photography, OCT, and staining of RPE/choroid flatmounts with anti-zonula occludens 1 (ZO-1) antibodies, a cell

Investigative Ophthalmology & Visual Science

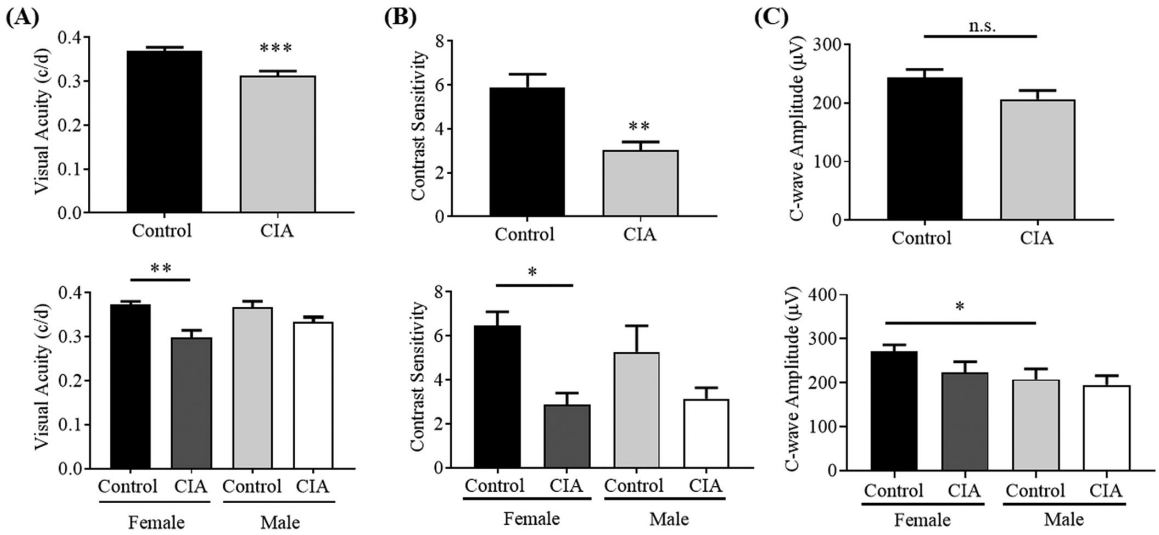

Figure 1. Analysis of visual function following collagen-induced arthritis. Optokinetic responses and ERG amplitudes were recorded 2 weeks following the induction of collagen-induced arthritis along with age-matched control mice. (**A**) Visual acuity was determined by measuring the spatial frequency threshold at a contrast of 100% and constant speed of 12°/s, where visual acuity was decreased in the CIA mice (n = 19–21 mice per condition). However, when mice were analyzed according to sex, only female mice had a significant decrease in visual acuity (n = 9–12 mice per sex and condition). (**B**) The reciprocal of the contrast threshold at a fixed spatial frequency (0.131 cyc/deg) and constant speed (12°/s) was used to measure contrast sensitivity. Here we observed a significant decrease in contrast sensitivity in the CIA mice (n = 19–24 mice per condition). Analysis according to sex again only demonstrated a significant difference between female control and CIA mice (n = 7–14 mice per sex and condition). (**C**) ERG analysis, determining c-wave amplitudes as a measure of RPE health, did not demonstrate any significant changes in response between the control and CIA mice, but a significant difference in c-wave amplitudes was observed between female and male control mice (n = 6–8 mice per sex and condition). Data are expressed as mean ± SEM (*$P \leq 0.05$, **$P \leq 0.001$, ***$P \leq 0.0001$).

junction marker. Here we observe both the control and CIA mice to have a healthy-looking fundus, and retinal thickness, as measured by OCT (Figs. 2A, 2B), was comparable between the two groups. Interestingly, sex-based differences were observed in the outer nuclear layer (ONL) of CIA but not control mice. In CIA, male mice had increased ONL thickness compared to females (Fig. 2B; $P \leq 0.05$). These differences in ONL thickness translated into differences in whole retina (WR) thickness, resulting in decreased WR thickness in female CIA mice compared to female controls (Fig. 2B; $P \leq 0.05$) and increased WR thickness in male CIA mice compared to male controls (Fig. 2B; $P \leq 0.05$). Male CIA mice also demonstrated a significant increase in WR thickness compared to CIA females ($P \leq 0.001$). Finally, RPE morphology was found to be unaffected by CIA, with normal cell area and hexagonal shape associated with healthy RPE observe in flatmounts of both control and CIA mice (Figs. 2C, 4E, 4F).

CNV Lesion Size Is Reduced in the Presence of CIA

The laser-induced CNV model is a well-characterized model for angiogenesis and fibrosis in wet AMD.[49] For our experiments, CNV was used in the presence and absence of CIA to evaluate the role of systemic inflammation on CNV size. Two weeks following the CIA booster injection, CNV was induced with four laser lesions around each optic nerve. On day 5 following laser, CNV lesion size was measured by OCT (Fig. 3A). Quantification of lesion size indicated a 30% decrease in CNV lesion size in CIA mice compared to the control mice (Fig. 3B; $P \leq 0.001$). Comparison between the sexes revealed a significant decrease in lesion sizes in the male CIA mice compared to the female CIA mice (Fig. 3B; $P \leq 0.05$), and within each sex, both female and male CIA mice had significantly smaller lesion sizes compared to their sex-matched controls ($P \leq 0.05$ and $P \leq 0.001$, respectively). No sex-based difference was observed for CNV lesion sizes in control mice (Fig. 3B). RPE function, determined by assessing c-wave responses, was not affected in an additive fashion. The c-wave amplitudes were not affected by CIA alone, and the drop in c-wave amplitude observed in CNV animals was driven mostly by females (female control mice compared to CNV alone and CIA + CNV; $P \leq 0.01$). Finally, as previously reported,[50] c-wave response amplitudes in untreated female mice were observed to be slightly higher than in male control mice ($P \leq 0.05$).

Increased $NaIO_3$-Induced Retinal Damage in the CIA Mice

There currently are no mouse models available to mimic every aspect of dry AMD. We chose to use the $NaIO_3$ model, a model resulting in photoreceptor damage by primarily affecting the RPE[51] and that has a timeline of induction/degeneration that can be overlaid with the CIA model. Two weeks following the CIA booster injection, mice were injected with 50 mg/kg $NaIO_3$. Ten days following $NaIO_3$ injection, retinal morphology and function were assessed (Fig. 4). Fundus photography demonstrated severe mottling of the RPE in $NaIO_3$-treated animals (Fig. 4A) compared to controls or CIA mice (Fig. 2A). While retinal thickness

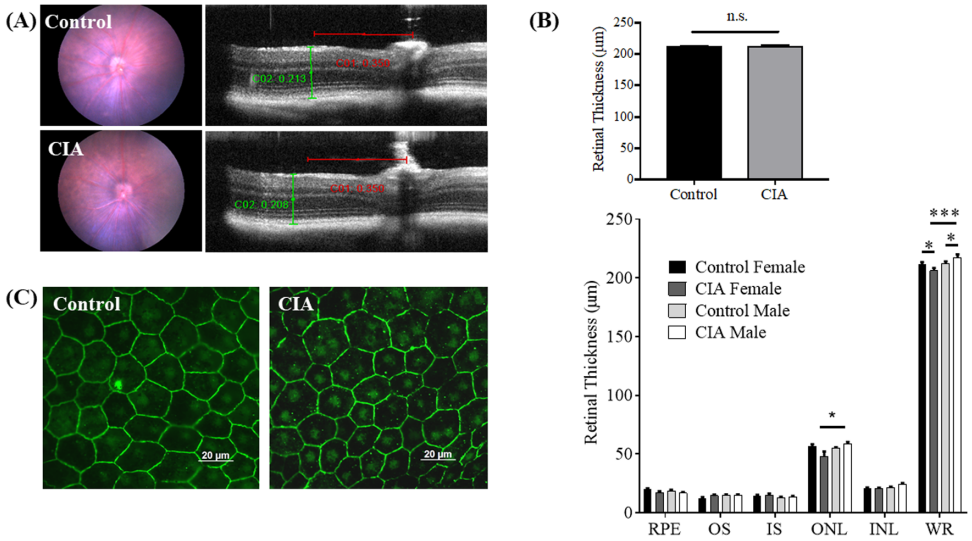

Figure 2. RPE and retina structure in the presence of CIA. (**A**) Representative fundus and OCT images demonstrated a similar appearance of the RPE and retina between CIA mice and control. (**B**) Measurements of retinal thickness showed no difference in WR between control and CIA mice (*top graph*). However, a separate analysis of the mice analyzed in **A** and **B** (*top graph*), grouped by sex (**B**, *bottom graph*), showed a significant difference between CIA female and male mice in ONL thickness (*$P \leq 0.05$). This difference is retained within the WR measurements, resulting in significant differences between the control and CIA for both female ($P = 0.0258$) and male (0.0172), as well as between CIA female and male (<0.0001). No significant differences were observed between the RPE, outer segment (OS), inner segment (IS), and inner nuclear layer (INL) measurements. (**C**) ZO-1 staining of control and CIA RPE/choroid flatmounts demonstrated healthy, hexagonally shaped RPE cells in both groups (see Figs. 4E and 4F for quantitative analysis). *Scale bar*: 20 µm. Data reported as ±SEM; n = 6–9 mice per sex and treatment group.

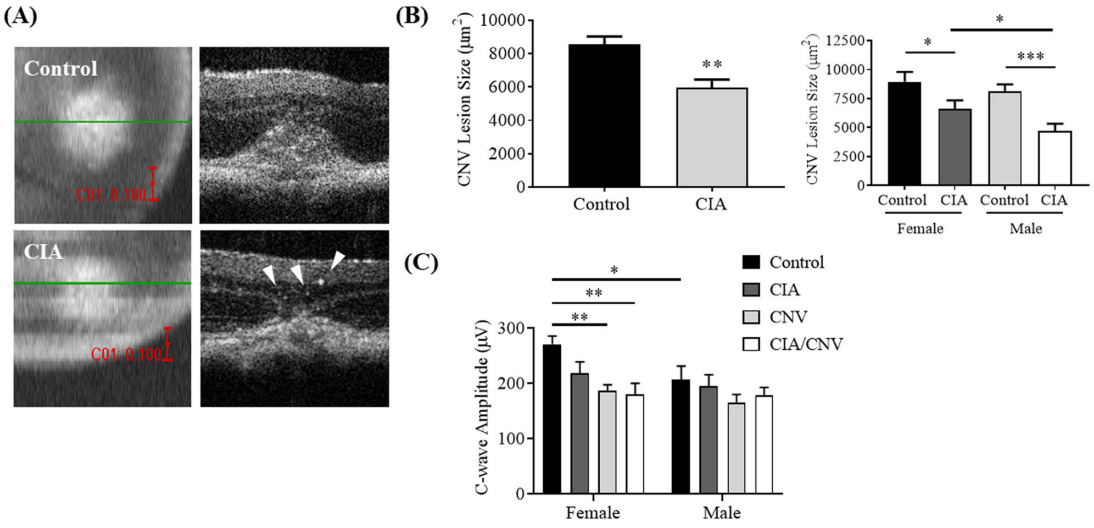

Figure 3. CNV is attenuated in the presence of CIA. Laser-induced CNV was induced in age-matched control and CIA mice in which arthritis had been induced by collagen immunization 4 to 5 weeks prior. On day 5 following laser, CNV was measured using OCT; RPE function was assessed by c-wave analysis. (**A**) Representative fundus (*en face*) and b-scan (*horizontal*) images, obtained by OCT demonstrate differences in CNV lesion size in CIA animals. *White arrowheads* point to hyperreflective spots observed in CIA mice. (**B**) Quantitative analysis of CNV images obtained by OCT demonstrated a significant decrease in CNV lesion size in CIA mice (**$P \leq 0.001$), as well as a significant difference between control female and CIA female mice (*$P \leq 0.05$) and control male versus CIA male mice (***$P = 0.0001$; n = 11–14 mice per sex and condition). (**C**) ERG analysis following CNV in the absence and presence of CIA demonstrated no significant differences between groups. Sex-based analysis revealed a higher c-wave amplitude at baseline for female mice (*$P \leq 0.05$) and significant changes between control and CNV and CIA + CNV (**$P \leq 0.01$), whereas few disease-associated changes were observed in males (n = 6–8 mice per sex and condition). Data shown are average values (±SEM) per lesion.

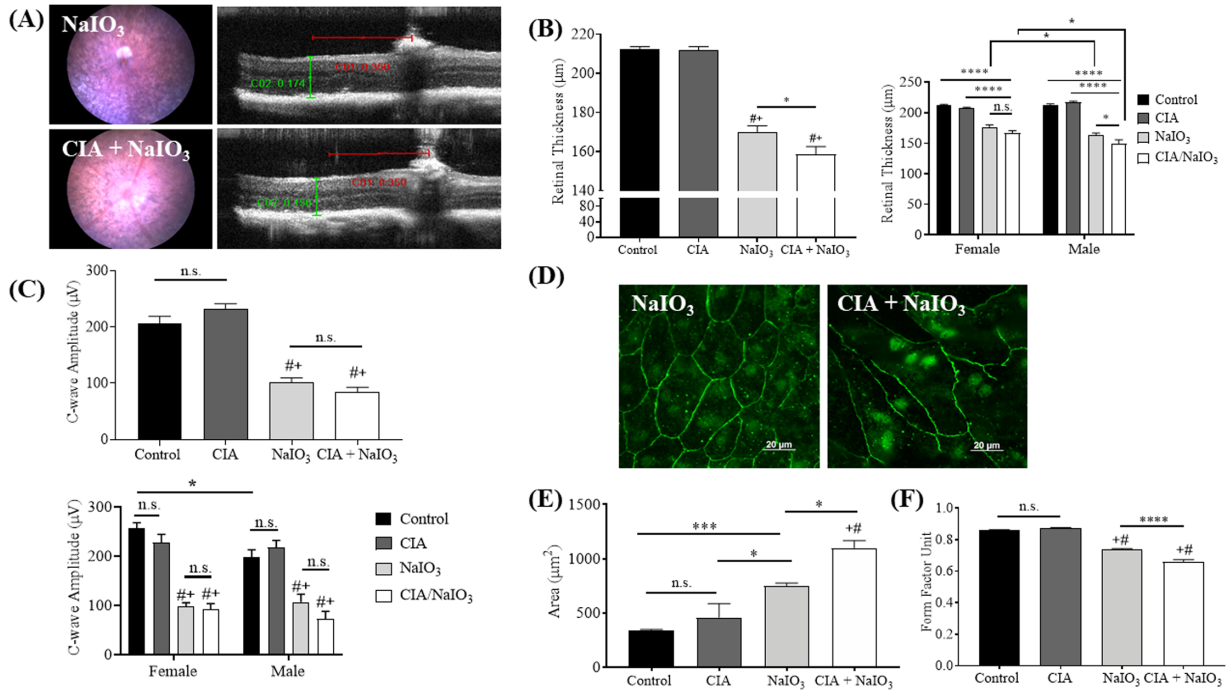

Figure 4. $NaIO_3$-induced retinal degeneration is aggravated in the presence of CIA. (**A**) Representative $NaIO_3$ and CIA + $NaIO_3$ images of fundus and OCT, documenting the mottled appearance of the fundus typical of RPE damage by $NaIO_3$, and an apparent thinning of the retina. (**B**) Quantitative analysis of retinal thickness shows a significant decrease in the CIA + $NaIO_3$ mice compared to $NaIO_3$ alone, and both were significantly reduced when compared to CIA alone or control mice (n = 11–16 mice). Analysis between male and female mice demonstrated that the significance between $NaIO_3$-treated and CIA + $NaIO_3$–treated mice was driven by the male mice. Male mice also had a greater decrease in retinal thickness in the $NaIO_3$ and CIA + $NaIO_3$ models compared to females. (**C**) The c-wave responses were significantly decreased in $NaIO_3$-treated mice compared to control and CIA mice. CIA + $NaIO_3$ mice also demonstrated a significant decrease in c-wave response compared to control and CIA. No significant (n.s.) differences between control and CIA or $NaIO_3$ and CIA + $NaIO_3$ groups were detected (n = 13–17 mice per group). Male mice were observed to have a significantly reduced c-wave amplitude compared to the female mice, while no additional sex differences in c-wave response were identified. (**D**) ZO-1 staining demonstrated a decrease in RPE health in the $NaIO_3$-treated mice, which was exacerbated in the presence of CIA. (**E**) A significant increase in RPE cell size was observed for $NaIO_3$-treated mice compared to either control or CIA mice. Cell size was further increased in CIA + $NaIO_3$–treated mice compared to control or CIA mice. No significant difference was observed between control and CIA mice. (**F**) Form factor (circularity) was decreased in the presence of $NaIO_3$ compared to control and CIA mice, with an additive decrease observed in CIA + $NaIO_3$–treated mice compared to $NaIO_3$ alone. No significant difference was observed between control and CIA mice (n = 5–7 mice per treatment condition for morphology analyses. Data are expressed as mean ± SEM (*$P \leq 0.05$, ***$P \leq 0.001$, ****$P \leq 0.0001$, $^{+}P \leq 0.0001$ compared to control, $^{\#}P \leq 0.0001$ compared to CIA). *Scale bar*: 20 µm.

again demonstrated no change between control and CIA mice alone, thickness was decreased by ~20% in $NaIO_3$-treated mice compared to controls. This decrease was further exacerbated by the presence of CIA, suggesting an additive effect (Figs. 4A, 4B; $P \leq 0.05$). Please note that the damage caused by $NaIO_3$ made it too difficult to discern the different layers of the retina for additional and more detailed quantifications. Retinal thickness between female and male mice was found to be significantly different between $NaIO_3$ ($P \leq 0.05$) and CIA + $NaIO_3$ mice ($P \leq 0.05$; Fig. 4B). However, a significant difference was observed only in the male mice between $NaIO_3$ and CIA + $NaIO_3$ ($P \leq 0.05$). ERG c-wave responses were also decreased in the presence of $NaIO_3$ and CIA + $NaIO_3$ compared to control and CIA mice (Fig. 4C; $P \leq 0.0001$). However, due to the greatly diminished c-wave response caused by $NaIO_3$, differences between $NaIO_3$ and CIA + $NaIO_3$ were indiscernible. These results were also true for c-wave comparisons made between sexes. However, as previously reported, c-wave responses in male mice were significantly lower than in female mice.[50] ZO-1 staining in the peripheral area of RPE/choroid flatmounts demonstrated a loss of normal RPE hexagonal shape documented in control and CIA mice (Fig. 2C) in the presence of $NaIO_3$ (Fig. 4D), indicative of a very unhealthy RPE, and damage that appeared to be further increased in the presence of CIA. Quantification of cell area (Fig. 4E) and form factor (Fig. 4F) was used to confirm these observations. Here we observed no significant difference between RPE cell area and form factor (a measurement of circularity) between control and CIA mice. Significant increases in cell area were observed in $NaIO_3$-treated mice compared to control ($P \leq 0.001$) and CIA ($P \leq 0.05$) mice (Fig. 4E). This increase in size was further augmented in CIA + $NaIO_3$ mice compared to control ($P \leq 0.0001$) and CIA ($P \leq 0.0001$). Importantly, CIA + $NaIO_3$ demonstrated an added increase in cell area compared to $NaIO_3$ alone ($P \leq 0.05$). Likewise, $NaIO_3$-treated and CIA + $NaIO_3$–treated mice both exhibited a decrease in RPE form factor compared to control ($P \leq 0.0001$) and CIA ($P \leq 0.0001$; Fig. 4F) mice, and an even greater decrease in form factor was found in CIA + $NaIO_3$ mice compared to $NaIO_3$ alone ($P \leq 0.0001$). These results indicate that $NaIO_3$ treatment leads to an increase in elongated cell size and loss of the normal hexagonal shape observed in healthy RPE cells, both of which are further

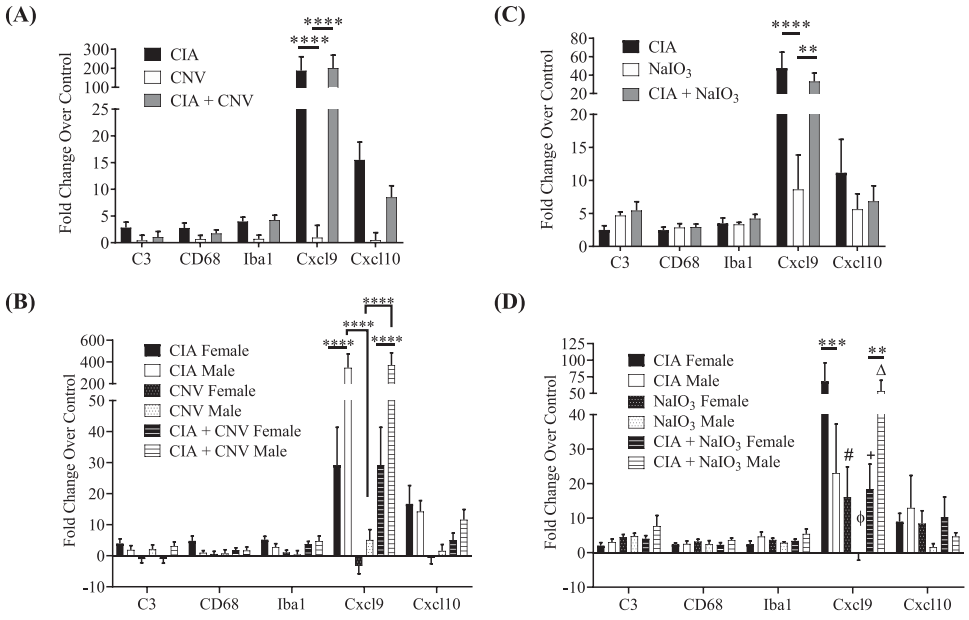

Figure 5. Analysis of mRNA expression of genes involved in inflammation. (**A**) mRNA expression analysis shows no significant change in gene fold expression in C3, CD68, Iba1, or Cxcl10 in the presence of CIA, CNV, or CIA + CNV. Significant differences for Cxcl9 fold expression were observed in CIA versus CNV, as well CIA versus CIA + CNV. (**B**) Gene expression comparison between the sexes shows a significant increase in Cxcl9 expression in CIA males compared to CIA females, as well as a significant increase in male CIA + CNV compared to female CIA + CNV. In addition, male mice had a significant decrease in CIA versus CNV and a significant increase in CNV versus CIA + CNV. (**C**) Mice treated with $NaIO_3$ in the presence and absence of CIA also demonstrated significant differences in Cxcl9 expression alone. Here we observed a significant decrease in Cxcl9 in the presence of $NaIO_3$ compared to CIA and an increase in expression in the presence of CIA +$NaIO_3$. (**D**) Analysis between the sexes in the $NaIO_3$ model demonstrated a significant decrease in Cxcl9 in the male CIA mice compared to the female CIA mice. Sex-related differences were also observed between male and female CIA + $NaIO_3$ mice, in which a significant increase in Cxcl9 was observed in the male mice. In addition, female CIA mice had a significant decrease in Cxcl9 in $NaIO_3$-treated and CIA + $NaIO_3$–treated mice. Male mice had a significant increase in Cxcl9 expression in CIA + $NaIO_3$–treated mice compared to male CIA and a decrease in $NaIO_3$-treated versus CIA + $NaIO_3$. Data are expressed as mean ± SEM with $n = 5$–8 mice per sex and condition (**$P \leq 0.01$, ***$P \leq 0.001$, ****$P \leq 0.0001$, $^{\#}P \leq 0.0001$ female: $NaIO_3$ versus CIA, $^{+}P \leq 0.0001$ female: CIA + $NaIO_3$ versus CIA, $^{\phi}P \leq 0.0001$ male: $NaIO_3$ versus CIA; $^{\Delta}P \leq 0.05$ male: CIA + $NaIO_3$ versus CIA).

increased in the presence of CIA. No significant differences were observed between sex (data not shown).

Increased Inflammatory Gene Expression in the Presence of CIA

Expression levels of genes involved in inflammatory responses were analyzed in both the CNV and $NaIO_3$ experimental models in the presence and absence of CIA. Here we measured fold change expression of complement component, C3; cluster of differentiation (CD) 68, a macrophage marker; ionized calcium-binding adapter molecule 1 (Iba1), a microglia/macrophage marker; and chemokine ligand 9 (Cxcl9) and C-X-C motif chemokine ligand 10 (Cxcl10), two chemokines sharing the receptor CXCR3. The selection of markers was based in part on the observation of pronounced hyperreflective spots surrounding the CNV lesions of the CIA mice (Fig. 3A). These hyperreflective spots have been suggested to be the result of increased inflammatory cell invasion, including macrophages,[52] potentially recruited by C3a anaphylatoxin production.[53] In addition, M1 macrophage-related markers tend to be upregulated in the early stages of disease in mouse models of AMD.[54]

While an approximately two- and fourfold increase in respective CD68 and Iba1 expression was observed in the CIA and CIA + CNV mice, no significance was observed compared to the CNV mice alone. No significant changes were observed in the $NaIO_3$ model or between sex in either model. These results, however, may be due in part to the time point when the RPE/choroid samples were collected (day 6 after CNV and day 11 after $NaIO_3$), as an earlier time point may have revealed significant changes in gene expression.

While C3 and Cxcl10 did not show significant differences in expression among the groups investigated, expression of Cxcl9 was greatly increased in CIA compared to CNV mice ($P \leq 0.0001$; Fig. 5A) and $NaIO_3$-treated mice ($P \leq 0.0001$; Fig. 5C). Cxcl9 levels, however, were driven by CIA only, since levels in CIA and CIA + CNV or CIA and CIA + $NaIO_3$ did not differ (n.s.). Analysis between the sexes revealed a significant difference in Cxcl9 expression levels between female CIA and male CIA mice. Samples collected from male CIA mice as part of the CNV experiment had a greater increase in Cxcl9 expression compared to female mice of the same cohort ($P \leq 0.0001$; Fig. 5B), whereas the reverse was true in CIA mice in the $NaIO_3$ test group ($P \leq 0.001$; Fig. 5D). Sex differences in Cxcl9 expression were also observed in CIA + CNV mice ($P \leq 0.0001$) and CIA + $NaIO_3$–treated mice ($P \leq 0.01$), both of which were found to exhibit increased expression levels in the male mice.

Discussion

The role of systemic inflammation AMD is largely unknown. In this present study, we used animal models for CNV and retinal degeneration and tested them in the presence of a second chronic condition, a model for rheumatoid arthritis. Using these models, we observed differences in the severity of CNV and retinal degeneration in the presence of systemic inflammation caused by collagen induced arthritis. Additionally, subtle differences in disease severity and gene expression were observed between male and female mice. Together, these results suggest that systemic inflammation may play a role in AMD pathology, which may be further exacerbated between the sexes.

The eye is considered a site of immune privilege, with characteristics that provide protection from inflammatory insult while also offering a site of therapeutic interest. Although this asset allows the eye to deter various stressors, immune privilege can be lost as the result of breaches to the blood-retinal barrier caused by injury and aging. As genetics and environment impact individual aging processes, so does chronic inflammation. Described as "inflammaging,"[55] chronically elevated levels of immune response and stress are believed to lead to greater comorbidity and mortality.[56] In addition to genetics and a healthy lifestyle, individuals who live longer lives are found to have increased levels of anti-inflammatory markers, while increased proinflammatory markers are associated with increased disease (as reviewed by Franceschi[57]). Our patient database analysis,[23] as well as studies performed by others, observed increased number of AMD cases in the presence of systemic disease, suggesting a role for inflammaging in AMD risk and pathogenesis.

As we previously identified an increased risk and earlier time of diagnosis of dry AMD among patients with RA,[23] we sought to investigate how systemic inflammation may affect disease severity in animal models of AMD. Using the CIA model for RA, the CNV laser-induced model to assess angiogenesis associated with wet AMD, and the $NaIO_3$-induced retinal degeneration model to model RPE and photoreceptor degeneration in dry AMD, we found that systemic inflammation affected AMD pathology differentially. CIA alone did not result in significant differences in RPE health as indicated by c-wave responses (ERG; Fig. 1) or RPE morphology (OCT, ZO-1; Fig. 2), but retinal function was impaired based on a reduction in visual acuity and contrast sensitivity. While the results on visual performance suggest a loss in retinal function, effects on subcortical circuits known to control the OKR response (diencephalon, the accessory optic system, pons, and dorsal medulla) cannot be excluded.[58] In CIA mice, significant changes in voluntary behavior have been reported,[59] as well as loss of locomotion and equilibrium,[60] all of which could affect the OKR response. In addition, in patients with RA, ocular manifestations include dry eye syndrome, episcleritis, scleritis, peripheral ulcerative keratitis,[61] and optic neuritis,[62,63] which can be associated with decreased visual acuity and contrast sensitivity; however, those pathologies were not tested in our mice.

RA has been associated with new vessel growth in the synovial tissues, involving cytokines such as TNF-α and IL-6 either directly or indirectly, stimulating the release of VEGF from synovial fibroblasts.[64] Since VEGF, TNF-α,[65] and IL-6[66] together and individually can promote CNV, we anticipated an increase in CNV lesion size in the presence of CIA. Therefore, we were surprised to see that, rather than an additive effect on CNV lesion size, we uncovered a significant decrease in lesion size by ~30% (Fig. 3). He and Marneros[67] reported an increase in monokine induced by IFNγ, also known as Cxcl9, expression in the presence of doxycycline, a broad-spectrum antibiotic found to decrease CNV.[68] This led us to examine Cxcl9 levels within our disease models. In addition, we examined expression of interferon γ inducible 10 kd, also known as Cxcl10. Both Cxcl9 and Cxcl10 are interferon-inducible CXC chemokine receptor 3 (CXCR3) ligands, and both have been found to have angiostatic properties.[69,70] In addition, Cxcl10 and Cxcl9 are found to inhibit neovascularization[60] and to be elevated in the fluid of patients with RA.[61] Also included in our molecular analysis were C3, CD68, and Iba1, inflammatory genes found to be increased in synovial fluid or tissue of patients with RA.[71–73] Of the genes tested, significance between disease groups and sex was only identified for Cxcl9 (Fig. 5). Here we observed a >100-fold increase in Cxcl9 expression in CIA mice over control mice and a similar increase in mice treated with CIA + CNV. Mice with CNV alone had no significant change in Cxcl9 expression (Fig. 5A). Similarly, Cxcl10 expression was also increased in the presence of CIA, but the differences did not reach statistical significance. Increased levels of Cxcl9 and Cxcl10 were also present in the $NaIO_3$ model of dry AMD (Fig. 5C). In addition, sex-specific differences were observed in Cxcl9 expression. Interestingly, samples collected from male CIA mice as part of the CNV experiment had a greater increase in Cxcl9 expression compared to female mice of the same cohort (Fig. 5B), whereas the reverse was true in CIA mice in the $NaIO_3$ test group (Fig. 5D). These observed differences may be due to the timing by which the RPE/choroid fractions were collected. Mice in the $NaIO_3$ treatment group were collected at a later time point than the CNV cohort (day 11 versus day 6) and therefore had a greater lapse of time between collagen treatment and tissue collection. Sex differences were also observed in the CIA mice in the presence of our AMD models for wet and dry AMD. Here we observed male mice with CIA + CNV (Fig. 5B) or CIA + $NaIO_3$ (Fig. 5D) had a greater increase in fold gene expression compared to female mice. These results suggest that the increased presence of Cxcl9 may be the reason why CNV lesion size is reduced in the presence of CIA and why CIA males are found to have a significantly smaller CNV lesion size than CNV females (Fig. 3B). In a previous study analyzing inflammation of the liver, testosterone treatment was found to suppress inflammation through the regulation of Cxcl9 and Cxcl10.[74] While the interaction of testosterone and Cxcl9 is one hypothesis that might explain our observed differences, this requires further experiments, by suppressing or supplementing sex-specific hormones.

While CIA did not provide an additive effect in the mouse CNV model, we did observe an additive effect in the $NaIO_3$-induced retinal degeneration model of AMD. Here we found that $NaIO_3$ in the presence of CIA further increased retinal degeneration based on retinal thickness than with $NaIO_3$ alone (Figs. 4A, 4B). Staining with ZO-1 also revealed increased damage to the RPE in the presence of CIA and $NaIO_3$, which was demonstrated by the severe loss of the normal hexagonal shape and the transition to an elongated, fibrotic cell shape (Figs. 4D–4F). These combined results in the CNV and retinal degeneration models correlate with our Marketscan analysis of Medicare patients, which identified an increased risk of dry AMD, and not wet AMD, in the presence of RA.[23] Together, these results suggest that systemic

Investigative Ophthalmology & Visual Science

inflammation and the corresponding immune response in CIA or RA affect pathology in dry and wet AMD differentially. While systemic inflammation in CIA or RA was partially protective and resulted in reduced choroidal neovascularization or no increased risk for wet AMD, respectively, CIA was found to augment RPE damage and loss of retinal thickness, and RA increased the risk for dry AMD. As CIA led to increased levels of Cxcl9 and Cxcl10 in mouse RPE/choroids, we suggest that these CIA-primed chemokines led to the different disease severities in the CNV and retinal degeneration models of AMD. In this context, it is important to note that Cxcl9 is both angiostatic as well as cytotoxic, reducing angiogenesis but also disrupting barrier function[75] and triggering epithelial-mesenchymal transition.[76] These intriguing results shed additional light on the complexities that secondary inflammatory diseases may have on the pathogenesis of AMD. In our future studies, we plan to further explore the role of chemokines in our disease models and the mechanism by which they alter disease severity and progression.

AMD and RA are two diseases with noted sex differences. Both diseases are found to be more prevalent among females. In general, testosterone is found to be anti-inflammatory and estrogen to be proinflammatory.[77] Immune responses in mice are also found to be associated with increased proinflammatory cytokine responses, T-cell proliferation, and antibody responses in females when compared to males (as reviewed by Klein and Flanagan[78]). Hence, we hypothesized that female mice might exhibit increased disease severity. What we did observe were slight differences between female and male mice for CNV lesion size, retinal thickness and c-wave amplitudes, and Cxcl9 gene expression. Differences between male and female ONL have been documented among healthy individuals, where mean thickness of ONL was reported to be greater in women than in men.[79] ONL thinning has previously been identified to correlate with loss of visual acuity[80] and visual field sensitivity[81] in patients with retinitis pigmentosa. In addition, patients with acute optic neuritis as the result of systemic autoimmune disease had changes in ONL + photoreceptor inner and outer segment thickness over time, an observation believed to be due to retinal inflammation.[82] In our analysis, we observed that females with CIA had a significantly thinner ONL compared to CIA males. This observed difference in ONL thickness may explain why only a significant decrease in both visual acuity and contrast sensitivity is present in the female CIA cohort. While these changes may appear minor, they provide additional clues to sex-based differences in inflammatory responses. Interestingly, the triggers for the disease models (CNV- and $NaIO_3$-induced retinal degeneration) had a more significant impact on the male mice compared to females for several of our analyses. This finding may be indicative of the timing of our experiments and the susceptibility of males to acute inflammation, which is what both of our models of CNV and retinal degeneration represent.

In summary, our data, demonstrating that systemic inflammation by CIA increased disease progression in a retinal degeneration model but reduced progression in a CNV model of AMD, correlate with our observation that RA in patients increases prevalence and accelerates onset of dry AMD but does not affect wet AMD risk. However, the observed differences in disease severity between female and male mice, which are opposite of that observed in human patients, highlight the need for future experiments, incorporating age and chronic mouse models of disease.

Acknowledgments

Supported by National Institutes of Health (NIH) K12HD055885 Building Interdisciplinary Research Careers in Women's Health (BIRCWH) fellowship and the Medical University of South Carolina College of Medicine institutional support (GS), NIH 2R56 AR051749–15 (NKB-CoI), and NIH (R01EY024581), the Department of Veterans Affairs (I01RX000444, I01BX003050, and IK6BX004858), and the South Carolina SmartState Endowment (BR).

Disclosure: **G. Schnabolk,** None; **E. Obert,** None; **N.K. Banda,** None; **B. Rohrer,** None

References

1. Klein RJ, Zeiss C, Chew EY, et al. Complement factor H polymorphism in age-related macular degeneration. *Science*. 2005;308(5720):385–389.
2. Edwards AO, Ritter R III, Abel KJ, Manning A, Panhuysen C, Farrer LA. Complement factor H polymorphism and age-related macular degeneration. *Science*. 2005;308(5720):421–424.
3. Hageman GS, Anderson DH, Johnson LV, et al. A common haplotype in the complement regulatory gene factor H (HF1/CFH) predisposes individuals to age-related macular degeneration. *Proc Natl Acad Sci USA*. 2005;102(20):7227–7232.
4. Haines JL, Hauser MA, Schmidt S, et al. Complement factor H variant increases the risk of age-related macular degeneration. *Science*. 2005;308(5720):419–421.
5. Gold B, Merriam JE, Zernant J, et al. Variation in factor B (BF) and complement component 2 (C2) genes is associated with age-related macular degeneration. *Nat Genet*. 2006;38(4):458–462.
6. McKay GJ, Silvestri G, Patterson CC, Hogg RE, Chakravarthy U, Hughes AE. Further assessment of the complement component 2 and factor B region associated with age-related macular degeneration. *Invest Ophthalmol Vis Sci*. 2009;50(2):533–539.
7. Fritsche LG, Loenhardt T, Janssen A, et al. Age-related macular degeneration is associated with an unstable ARMS2 (LOC387715) mRNA. *Nat Genet*. 2008;40(7):892–896.
8. Yang Z, Camp NJ, Sun H, et al. A variant of the HTRA1 gene increases susceptibility to age-related macular degeneration. *Science*. 2006;314(5801):992–993.
9. Dewan A, Liu M, Hartman S, et al. HTRA1 promoter polymorphism in wet age-related macular degeneration. *Science*. 2006;314(5801):989–992.
10. Yates JR, Sepp T, Matharu BK, et al. Genetic factors in AMDSG: complement C3 variant and the risk of age-related macular degeneration. *N Engl J Med*. 2007;357(6):553–561.
11. McCarty CA, Mukesh BN, Fu CL, Mitchell P, Wang JJ, Taylor HR. Risk factors for age-related maculopathy: the Visual Impairment Project. *Arch Ophthalmol*. 2001;119(10):1455–1462.
12. Parekh N, Voland RP, Moeller SM, et al. Association between dietary fat intake and age-related macular degeneration in the Carotenoids in Age-Related Eye Disease Study (CAREDS): an ancillary study of the Women's Health Initiative. *Arch Ophthalmol*. 2009;127(11):1483–1493.
13. Jonas JB, Cheung CMG, Panda-Jonas S. Updates on the epidemiology of age-related macular degeneration. *Asia Pac J Ophthalmol*. 2017;6(6):493–497.
14. Smith W, Mitchell P, Wang JJ. Gender, oestrogen, hormone replacement and age-related macular degeneration: results from the Blue Mountains Eye Study. *Aust N Z J Ophthalmol*. 1997;25(suppl 1):S13–S15.

15. National Eye Institute. Age-related macular degeneration (AMD) data and statistics. Available at: https://www.nei.nih.gov/learn-about-eye-health/resources-for-health-educators/eye-health-data-and-statistics/age-related-macular-degeneration-amd-data-and-statistics. Accessed July 17, 2019.
16. Yannuzzi LA, Negrão S, Iida T, et al. Retinal angiomatous proliferation in age-related macular degeneration. *Retina*. 2001;21(5):416–434.
17. Cohen SY, Creuzot-Garcher C, Darmon J, et al. Types of choroidal neovascularisation in newly diagnosed exudative age-related macular degeneration. *Br J Ophthalmol*. 2007;91(9):1173–1176.
18. Massacesi AL, Sacchi L, Bergamini F, Bottoni F. The prevalence of retinal angiomatous proliferation in age-related macular degeneration with occult choroidal neovascularization. *Graefes Arch Clin Exp Ophthalmol*. 2008;246(1):89–92.
19. Singh JA, Cleveland JD. Gout and the risk of age-related macular degeneration in the elderly. *PLoS One*. 2018;13(7):e0199562.
20. Chen X, Rong SS, Xu Q, et al. Diabetes mellitus and risk of age-related macular degeneration: a systematic review and meta-analysis. *PLoS One*. 2014;9(9):e108196.
21. Wang J, Xue Y, Thapa S, Wang L, Tang J, Ji K. Relation between age-related macular degeneration and cardiovascular events and mortality: a systematic review and meta-analysis. *BioMed Res Int*. 2016;2016:8212063.
22. Bak M, Sorensen TL, Flachs EM, et al. Age-related macular degeneration in patients with chronic myeloproliferative neoplasms. *JAMA Ophthalmol*. 2017;135(8):835–843.
23. Schnabolk G, Rohrer B, Simpson KN. Increased nonexudative age-related macular degeneration diagnosis among Medicare beneficiaries with rheumatoid arthritis. *Invest Ophthalmol Vis Sci*. 2019;60(10):3520–3526.
24. Hunter TM, Boytsov NN, Zhang X, Schroeder K, Michaud K, Araujo AB. Prevalence of rheumatoid arthritis in the United States adult population in healthcare claims databases, 2004–2014. *Rheumatol Int*. 2017;37(9):1551–1557.
25. Ruddy S, Colten HR. Rheumatoid arthritis. Biosynthesis of complement proteins by synovial tissues. *N Engl J Med*. 1974;290(23):1284–1288.
26. Olmez U, Garred P, Mollnes TE, Harboe M, Berntzen HB, Munthe E. C3 activation products, C3 containing immune complexes, the terminal complement complex and native C9 in patients with rheumatoid arthritis. *Scand J Rheumatol*. 1991;20(3):183–189.
27. Morgan BP, Daniels RH, Williams BD. Measurement of terminal complement complexes in rheumatoid arthritis. *Clin Exp Immunol*. 1988;73(3):473–478.
28. Anderson DH, Radeke MJ, Gallo NB, et al. The pivotal role of the complement system in aging and age-related macular degeneration: hypothesis re-visited. *Prog Retin Eye Res*. 2010;29(2):95–112.
29. Rezar-Dreindl S, Sacu S, Eibenberger K, et al. The intraocular cytokine profile and therapeutic response in persistent neovascular age-related macular degeneration. *Invest Ophthalmol Vis Sci*. 2016;57(10):4144–4150.
30. Liu B, Wei L, Meyerle C, et al. Complement component C5a promotes expression of IL-22 and IL-17 from human T cells and its implication in age-related macular degeneration. *J Transl Med*. 2011;9:1–12.
31. Oh H, Takagi H, Takagi C, et al. The potential angiogenic role of macrophages in the formation of choroidal neovascular membranes. *Invest Ophthalmol Vis Sci*. 1999;40(9):1891–1898.
32. Okamoto H, Hoshi D, Kiire A, Yamanaka H, Kamatani N. Molecular targets of rheumatoid arthritis. *Inflamm Allergy Drug Targets*. 2008;7(1):53–66.
33. Medzhitov R. Origin and physiological roles of inflammation. *Nature*. 2008;454(7203):428–435.
34. Banda NK, Kraus DM, Muggli M, Bendele A, Holers VM, Arend WP. Prevention of collagen-induced arthritis in mice transgenic for the complement inhibitor complement receptor 1-related gene/protein y. *J Immunol*. 2003;171(4):2109–2115.
35. Banda NK, Kraus D, Vondracek A, et al. Mechanisms of effects of complement inhibition in murine collagen-induced arthritis. *Arthritis Rheum*. 2002;46(11):3065–3075.
36. Banda NK, Vondracek A, Kraus D, et al. Mechanisms of inhibition of collagen-induced arthritis by murine IL-18 binding protein. *J Immunol*. 2003;170(4):2100–2105.
37. Prusky GT, Alam NM, Beekman S, Douglas RM. Rapid quantification of adult and developing mouse spatial vision using a virtual optomotor system. *Invest Ophthalmol Vis Sci*. 2004;45(12):4611–4616.
38. Woodell A, Coughlin B, Kunchithapautham K, et al. Alternative complement pathway deficiency ameliorates chronic smoke-induced functional and morphological ocular injury. *PLoS One*. 2013;8(6):e67894.
39. Ablonczy Z, Crosson CE. VEGF modulation of retinal pigment epithelium resistance. *Exp Eye Res*. 2007;85(6):762–771.
40. Schnabolk G, Stauffer K, O'Quinn E, Coughlin B, Kunchithapautham K, Rohrer B. A comparative analysis of C57BL/6J and 6N substrains; chemokine/cytokine expression and susceptibility to laser-induced choroidal neovascularization. *Exp Eye Res*. 2014;129:18–23.
41. Giani A, Thanos A, Roh MI, et al. In vivo evaluation of laser-induced choroidal neovascularization using spectral-domain optical coherence tomography. *Invest Ophthalmol Vis Sci*. 2011;52(6):3880–3887.
42. Schnabolk G, Parsons N, Obert E, et al. Delivery of CR2-fH using AAV vector therapy as treatment strategy in the mouse model of choroidal neovascularization. *Mol Ther Methods Clin Dev*. 2018;9:1–11.
43. Obert E, Strauss R, Brandon C, et al. Targeting the tight junction protein, zonula occludens-1, with the connexin43 mimetic peptide, alphaCT1, reduces VEGF-dependent RPE pathophysiology. *J Mol Med (Berl)*. 2017;95(5):535–552.
44. Nozaki M, Raisler BJ, Sakurai E, et al. Drusen complement components C3a and C5a promote choroidal neovascularization. *Proc Natl Acad Sci USA*. 2006;103(7):2328–2333.
45. Rohrer B, Long Q, Coughlin B, et al. A targeted inhibitor of the alternative complement pathway reduces angiogenesis in a mouse model of age-related macular degeneration. *Invest Ophthalmol Vis Sci*. 2009;50(7):3056–3064.
46. Chowers G, Cohen M, Marks-Ohana D, et al. Course of sodium iodate-induced retinal degeneration in albino and pigmented mice. *Invest Ophthalmol Vis Sci*. 2017;58(4):2239–2249.
47. Coughlin B, Schnabolk G, Joseph K, et al. Connecting the innate and adaptive immune responses in mouse choroidal neovascularization via the anaphylatoxin C5a and gammadeltaT-cells. *Sci Rep*. 2016;6:23794.
48. Akamine R, Yamamoto T, Watanabe M, et al. Usefulness of the 5' region of the cDNA encoding acidic ribosomal phosphoprotein P0 conserved among rats, mice, and humans as a standard probe for gene expression analysis in different tissues and animal species. *J Biochem Biophys Methods*. 2007;70(3):481–486.
49. Pennesi ME, Neuringer M, Courtney RJ. Animal models of age related macular degeneration. *Mol Aspects Med*. 2012;33(4):487–509.
50. Schnabolk G, Obert E, Rohrer B. Sex related differences in retinal pigment epithelium and retinal disease. In: Klettner AK, Dithmar S, eds. *Retinal Pigment Epithelium in*

Health and Disease. Cham, Switzerland: Springer International; 2020:185–201.

51. Kiuchi K, Yoshizawa K, Shikata N, Moriguchi K, Tsubura A. Morphologic characteristics of retinal degeneration induced by sodium iodate in mice. *Curr Eye Res*. 2002;25(6):373–379.
52. Kokona D, Häner NU, Ebneter A, Zinkernagel MS. Imaging of macrophage dynamics with optical coherence tomography in anterior ischemic optic neuropathy. *Exp Eye Res*. 2017;154:159–167.
53. Markiewski MM, Lambris JD. The role of complement in inflammatory diseases from behind the scenes into the spotlight. *Am J Pathol*. 2007;171(3):715–727.
54. Cruz-Guilloty F, Saeed AM, Echegaray JJ, et al. Infiltration of proinflammatory M1 macrophages into the outer retina precedes damage in a mouse model of age-related macular degeneration. *Int J Inflamm*. 2013;2013:503725.
55. Franceschi C, Bonafè M, Valensin S, et al. Inflamm-aging: an evolutionary perspective on immunosenescence. *Ann N Y Acad Sci*. 2000;908:244–254.
56. Divo MJ, Martinez CH, Mannino DM. Ageing and the epidemiology of multimorbidity. *Eur Respir J*. 2014;44(4):1055–1068.
57. Franceschi C. Inflammaging as a major characteristic of old people: can it be prevented or cured? *Nutr Rev*. 2007;65(12, pt 2):S173–S176.
58. Cahill H, Nathans J. The optokinetic reflex as a tool for quantitative analyses of nervous system function in mice: application to genetic and drug-induced variation. *PLoS One*. 2008;3(4):e2055.
59. Oto Y, Takahashi Y, Kurosaka D, Kato F. Alterations of voluntary behavior in the course of disease progress and pharmacotherapy in mice with collagen-induced arthritis. *Arthritis Res Ther*. 2019;21(1):284.
60. Mausset-Bonnefont AL, Cren M, Vicente R, et al. Arthritis sensory and motor scale: predicting functional deficits from the clinical score in collagen-induced arthritis. *Arthritis Res Ther*. 2019;21(1):264.
61. Generali E, Cantarini L, Selmi C. Ocular involvement in systemic autoimmune diseases. *Clin Rev Allergy Immunol*. 2015;49(3):263–270.
62. Ağildere AM, Tutar NU, Yücel E, Coşkun M, Benli S, Aydin P. Pachymeningitis and optic neuritis in rheumatoid arthritis: MRI findings. *Br J Radiol*. 1999;72(856):404–407.
63. Chen YH, Wang AG, Lin YC, Yen MY. Optic neuritis as the first manifestation of rheumatoid arthritis. *J Neuroophthalmol*. 2008;28(3):237–238.
64. Szekanecz Z, Koch AE. Angiogenesis and its targeting in rheumatoid arthritis. *Vasc Pharmacol*. 2009;51(1):1–7.
65. Shi X, Semkova I, Muther PS, Dell S, Kociok N, Joussen AM. Inhibition of TNF-alpha reduces laser-induced choroidal neovascularization. *Exp Eye Res*. 2006;83(6):1325–1334.
66. Izumi-Nagai K, Nagai N, Ozawa Y, et al. Interleukin-6 receptor-mediated activation of signal transducer and activator of transcription-3 (STAT3) promotes choroidal neovascularization. *Am J Pathol*. 2007;170(6):2149–2158.
67. He L, Marneros AG. Doxycycline inhibits polarization of macrophages to the proangiogenic M2-type and subsequent neovascularization. *J Biol Chem*. 2014;289(12):8019–8028.
68. Samtani S, Amaral J, Campos MM, Fariss RN, Becerra SP. Doxycycline-mediated inhibition of choroidal neovascularization. *Invest Ophthalmol Vis Sci*. 2009;50(11):5098–5106.
69. Strieter RM, Kunkel SL, Arenberg DA, Burdick MD, Polverini PJ. Interferon gamma-inducible protein 10 (IP-10), a member of the C-X-C chemokine family, is an inhibitor of angiogenesis. *Biochem Biophys Res Commun*. 1995;210(1):51–57.
70. Angiolillo AL, Sgadari C, Taub DD, et al. Human interferon-inducible protein 10 is a potent inhibitor of angiogenesis in vivo. *J Exp Med*. 1995;182(1):155–162.
71. Moxley G, Ruddy S. Elevated C3 anaphylatoxin levels in synovial fluids from patients with rheumatoid arthritis. *Arthritis Rheum*. 1985;28(10):1089–1095.
72. Bresnihan B, Pontifex E, Thurlings RM, et al. Synovial tissue sublining CD68 expression is a biomarker of therapeutic response in rheumatoid arthritis clinical trials: consistency across centers. *J Rheumatol*. 2009;36(8):1800.
73. Kimura M, Kawahito Y, Obayashi H, et al. A critical role for allograft inflammatory factor-1 in the pathogenesis of rheumatoid arthritis. *J Immunol*. 2007;178(5):3316.
74. Schwinge D, Carambia A, Quaas A, et al. Testosterone suppresses hepatic inflammation by the downregulation of IL-17, Cxcl-9, and Cxcl-10 in a mouse model of experimental acute cholangitis. *J Immunol*. 2015;194(6):2522–2530.
75. Amatschek S, Lucas R, Eger A, et al. Cxcl9 induces chemotaxis, chemorepulsion and endothelial barrier disruption through CXCR3-mediated activation of melanoma cells. *Br J Cancer*. 2011;104(3):469–479.
76. Li Z, Liu J, Li L, et al. Epithelial mesenchymal transition induced by the Cxcl9/CXCR3 axis through AKT activation promotes invasion and metastasis in tongue squamous cell carcinoma. *Oncol Rep*. 2018;39(3):1356–1368.
77. Klein SL. Hormonal and immunological mechanisms mediating sex differences in parasite infection. *Parasite Immunol*. 2004;26(6-7):247–264.
78. Klein SL, Flanagan KL. Sex differences in immune responses. *Nat Rev Immunol*. 2016;16(10):626–638.
79. Won JY, Kim SE, Park YH. Effect of age and sex on retinal layer thickness and volume in normal eyes. *Medicine*. 2016;95(46):e5441.
80. Sousa K, Fernandes T, Gentil R, Mendonça L, Falcão M. Outer retinal layers as predictors of visual acuity in retinitis pigmentosa: a cross-sectional study. *Graefes Arch Clin Exp Ophthalmol*. 2019;257(2):265–271.
81. Sayo A, Ueno S, Kominami T, et al. Significant relationship of visual field sensitivity in central 10° to thickness of retinal layers in retinitis pigmentosa. *Invest Ophthalmol Vis Sci*. 2018;59(8):3469–3475.
82. Al-Louzi OA, Bhargava P, Newsome SD, et al. Outer retinal changes following acute optic neuritis. *Multiple Sclerosis*. 2016;22(3):362–372.

Investigative Ophthalmology & Visual Science